C. Tracking Efficiencies and Carbon Luminosity Scans

1. Tracking in F_π-1 and F_π-2

The tracking efficiency is defined (8) as the ratio of events that should pass through the drift chambers, to the number of events for which an actual track is found. The fraction of events expected to pass through the drift chambers is extracted from a fiducial area where the scintillator paddles presented the highest hit efficiency.

The tracking efficiency depends on both the drift chamber hit efficiency and the tracking algorithm used in finding the track. From previous experiments, we know that the efficiency for tracking electrons through the HMS falls linearly with rates, due mainly to the presence of multiple tracks in the drift chambers at high rates. In order to accurately calculate the tracking efficiency, we applied tight particle identification (PID) requirements to select a pure data sample. These requirements are stricter than those used in the regular analysis. In the HMS, the particle identification requirements used to select pions in the tracking efficiency calculation consisted of cuts on the gas Cerenkov and the calorimeter for F_π-1 data, while for F_π-2 an additional cut on the aerogel Cerenkov was applied.

As already mentioned, one of the objectives of this effort was to align both of the F_π-1 and F_π-2 experimental data sets to the same level of reconstruction and analysis. For the first pass reconstruction of the F_π-1 data set, a tracking algorithm was used that did not address multiple track events. Since the π^- data are taken at high rates under the condition of potentially high electron contamination, this deficiency in the tracking algorithm could affect the accurate determination of the π^-/π^+ ratios. Thus, it was decided to reanalyze the F_π-1 data using the new tracking algorithm (5) used for the F_π-2 data set reconstruction. The newly (2003) redesigned tracking algorithm does a significantly better job in selecting the best one of several tracks (multiple tracks) per event than the older version. After adapting the analysis package to accept the format of the older F_π-1 data, the various analysis parameters characteristic to F_π-1 were used in the redesigned reconstruction software, as appropriate.

In the initial tracking efficiency analysis (used in F_π-1), the routine Analyzer/HTRACKING/h_track_tests.f incorporated cuts to exclude multiple good PMT ADC signals within the fiducial region of any hodoscope plane.

The specific lines implementing these cuts are:

```
do i=1,hxloscin(1)-1
if (hscinhit(1,i).EQ.1) hhitsweet1x=-1
```

```
enddo
do i=hxhiscin(1)+1,hscin_1x_nr
if (hscinhit(1,i).EQ.1) hhitsweet1x=-1
enddo

do i=1,hxloscin(2)-1
if (hscinhit(3,i).EQ.1) hhitsweet2x=-1
enddo
do i=hxhiscin(2)+1,hscin_2x_nr
if (hscinhit(3,i).EQ.1) hhitsweet2x=-1
enddo

do i=1,hyloscin(1)-1
if (hscinhit(2,i).EQ.1) hhitsweet1y=-1
enddo
do i=hyhiscin(1)+1,hscin_1y_nr
if (hscinhit(2,i).EQ.1) hhitsweet1y=-1
enddo

do i=1,hyloscin(2)-1
if (hscinhit(4,i).EQ.1) hhitsweet2y=-1
enddo
do i=hyhiscin(2)+1,hscin_2y_nr
if (hscinhit(4,i).EQ.1) hhitsweet2y=-1
enddo

if (abs(sweet1xscin-sweet2xscin).gt.3) hgoodscinhits=0
if (abs(sweet1yscin-sweet2yscin).gt.2) hgoodscinhits=0
```

In the case where there were multiple tracks in the same scintillator plane, these cuts place a bias on the event sample used to calculate the HMS tracking efficiency. Since 2-track events have lower efficiencies than 1-track events, the resulting bias caused the tracking efficiencies to be over estimated. We will call this first method of selecting the data sample the "old" tracking

efficiency method. For the F_π-2 hydrogen analysis, the above lines were commented out, removing the requirement of rejecting additional PMT hits outside the fiducial region and resulting in a "dirty" data sample which included multiple track events. We will call this later method the "new" tracking efficiency method.

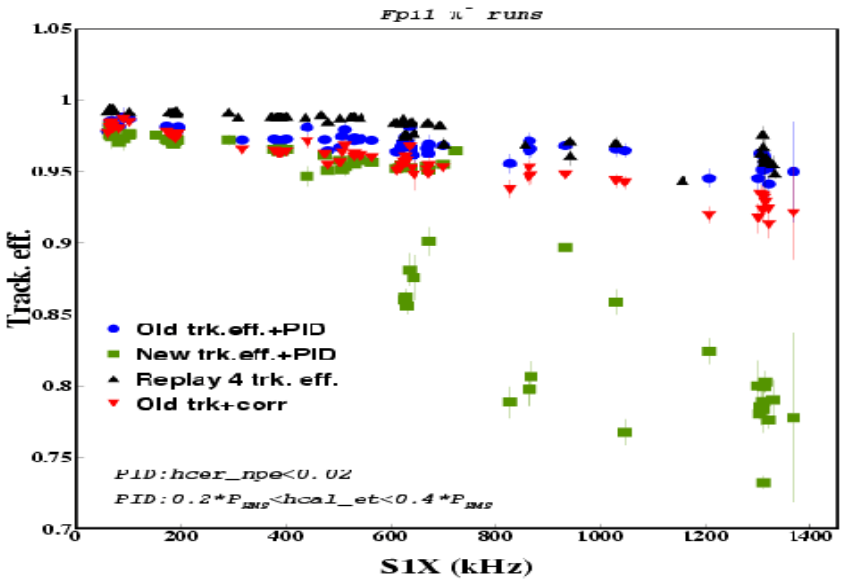

FIG. 7 F_π-1 tracking efficiencies extracted using the "new" (green squares) and "old" (blue dots) methods, plotted as a function of rates. Also shown are the over estimated tracking efficiencies obtained during the first F_π-1 analysis in 1998 (so called "replay 4" in black triangles), and the tracking efficiencies obtained with the "old" recipe plus a rate dependent correction which accounts for the fact that the ^{12}C should present no boiling effect (red upside down triangles).

The "new" tracking efficiency method, with the bias against multiple track events removed, was compared to the "old" tracking efficiency method for both the F_π-1 and F_π-2 π^- deuterium data sets. When making this comparison, it is important to note that the maximum rate encountered in the F_π-1 experiment was 1.3 MHz, while in F_π-2 (benefiting from the operational experience of the first experiment) the maximum rate was limited to 600 kHz. Thus, the F_π-1 deuterium data are much more sensitive to high rate tracking issues than the F_π-2 data.

F_π-1 tracking efficiencies were extracted using the "old" and "new" tracking efficiency methods described above, and they are shown as a function of rates in Fig. 7. The blue dots indicate the tracking efficiencies obtained using the prescription of the "old" tracking efficiency method plus PID cuts, while the green squares indicate the efficiencies obtained with the "new" recipe plus PID cuts. Also shown (black triangles) are the initial tracking efficiencies obtained during the last pass of analysis back in 1998, so called "replay 4". Clearly, they were over estimated. The red upside down triangles show the tracking efficiencies obtained using the "old" method, plus a rate

dependent correction which will be explained later in this section. For the case of the F_π-1 π^- data set, it can be seen (Fig. 7) that the "new" tracking efficiency method compares nicely with the "old" method up to rates ≈ 600 kHz, but fails for high rates (> 600 kHz). The "old" method appears to do a fairly good job in describing the expected fall of tracking efficiencies with rates.

2. F_π-2 Carbon Rate Studies

To obtain a better understanding of the HMS tracking efficiencies, a study of yields from carbon target versus rate and current was performed. In F_π-2, special luminosity scans using different beam currents and different targets (carbon, hydrogen and deuterium) were used to investigate rate and current dependent effects. Due to its very high boiling temperature (4554 K), the normalized yields from the carbon target should present no significant current or rate dependence if the various efficiencies are calculated correctly. Unfortunately, no ^{12}C luminosity scans were taken at different beam currents in the F_π-1 experiment, so any conclusions obtained from the F_π-2 study will have to be applied also to the F_π-1 data.

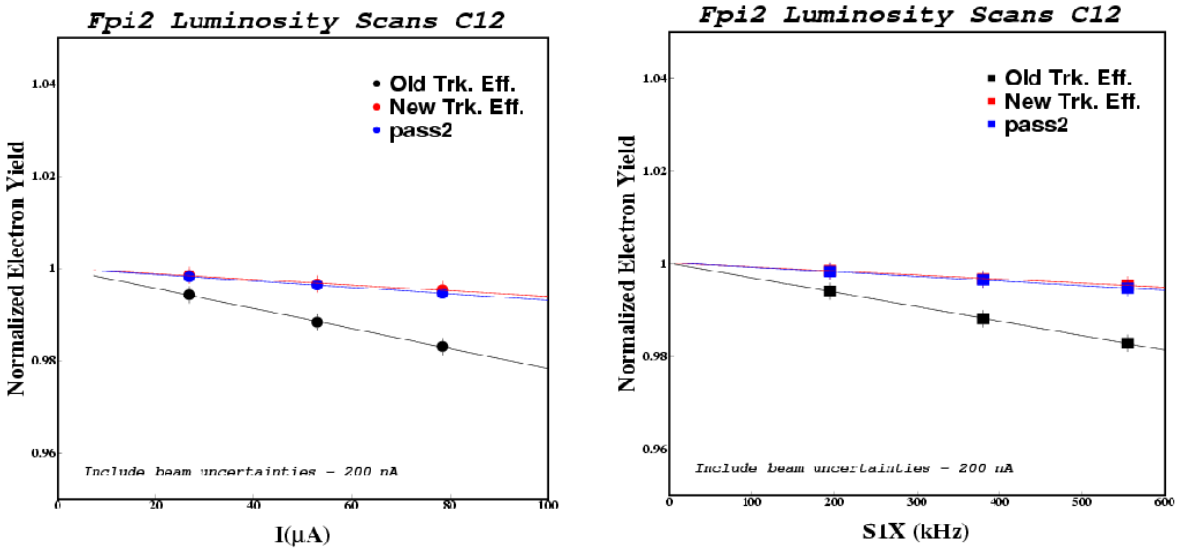

FIG. 8 Normalized $C(e,e')$ yields versus current and rate taken during the F_π-2 experiment. Since carbon targets are insensitive to beam heating effects at high current, the plot of yields versus current should be a horizontal line if all rate dependent effects are correctly taken into account in the data analysis. It is seen that the "new" tracking efficiencies do a better job at high rates than the "old" tracking efficiencies.

We compared the "new" tracking efficiencies to the scaler-based luminosity scans, which are independent of the tracking algorithm. Carbon runs were used to establish if the "new" tracking efficiency would have been consistent with the expected non-boiling effect of a solid target (related to beam current intensity dependence of normalized electron yields). Using tight PID cuts for

electrons detected in the HMS, we extracted the normalized yields as a function of beam current, using the form:

$$N_{yields} = \frac{N_e * PS1}{Q_{el} * El_{dt} * CPU_{dt} * Trk_{eff}}, \tag{8}$$

where N_e is the number of electrons obtained using PID cuts, $PS1$ is the prescaling factor applied during the data acquisition, Q_{el} is the accumulated charge, El_{dt} is the electron dead time, CPU_{dt} is the computer dead time, and Trk_{eff} is the tracking efficiency obtained using the scaler information and the prescription given by the "old" or "new" methods described earlier. The beam current dependence of normalized yields (including a 200 nA beam current uncertainty due to an offset in the beam current calibration) is shown in Fig. 8.

From Fig. 7, one can see that the "old" method of extracting tracking efficiencies does a better job for rates higher than 1 MHz, as is the case of the F_π-1 data set, while for rates lower than 600 MHz the "new" method of selecting the data sample for tracking efficiency is better suited. However, Fig. 8 indicates that the "new" method of extracting tracking efficiencies (which as well includes the improved tracking algorithm) is better as far as the F_π-2 carbon luminosity scans are concerned. Yet, when the tracking efficiency corrections calculated with the "old" method are inserted into Eqn. 8, a larger effect is observed than when the "new" method efficiencies are used. Since the "old" method for computing the tracking efficiencies is needed for the F_π-1 data set, it is necessary to implement a rate-dependent correction to the "old" method tracking efficiencies. This correction will be applied to both the F_π-1 and F_π-2 π^- data.

To carefully determine this correction to the "old" tracking efficiencies, a second study was performed incorporating a greater number of carbon runs taken in two different kinematic settings. Since the probability of a second particle traversing the HMS during the event resolving time is greater at high rates, it is likely that tight electron PID cuts will cause the rate dependence to be underestimated. Therefore only the following cuts

$$abs(hsdelta) < 8.5 \qquad abs(hsytar) < 5 \qquad abs(hsxptar) < 0.08 \qquad abs(hsyptar) < 0.05 \tag{9}$$

were applied in the second ntuples study, resulting in the data tabulated in Table I.

Normalized yields from the carbon target were computed using Eqn. 8 and the "old" (htr1) tracking efficiencies in Table I. They are plotted versus rate in Fig. 9. The error bars include statistical uncertainties and an estimated systematic uncertainty of 0.3% added in quadrature, to take into account beam steering on the target and other sensitive effects when no PID cut is applied. Data from the two kinematic settings were separately fit versus rate (blue and red curves

Run	Q_{tot}	hELLO	hS1X	BOT	PS1	htr1	htr2	cpult	hele	SING
$E_e = 4.210$ GeV, $\theta_{HMS} = 12.00$, $P_{HMS} = -3.000$										
47012	100621	181614321	279010493	1106.5	697.9	0.9775	0.8781	0.9671	0.9879	168963
47017	44330	80184449	123248274	608.5	299.3	0.9794	0.8822	0.9425	0.9903	170741
47018	31249	56737629	87321171	600.5	199.7	0.9802	0.8844	0.9394	0.9931	180750
47023	28692	52272441	80556749	923.5	199.8	0.9827	0.8882	0.9607	0.9959	171278
$E_e = 4.702$ GeV, $\theta_{HMS} = 10.57$, $P_{HMS} = -4.050$										
47757	42974	233316132	303696380	575.5	496.4	0.9687	0.9261	0.6415	0.9705	223257
47758	52953	301225113	373411559	660.5	992.4	0.9687	0.9242	0.7730	0.9693	165871
47759	124775	675461151	880596706	1590.5	1985.1	0.9685	0.9243	0.8738	0.9700	220334
47760	19126	107791771	138777445	710.5	249.3	0.9788	0.9059	0.7171	0.9896	233050
47763	56962	308207310	402136284	724.5	744.4	0.9690	0.8896	0.7225	0.9699	221788
47764	29473	160260551	209175826	376.5	248.2	0.9689	0.9236	0.4685	0.9701	221964

TABLE I HMS carbon luminosity study data taken during F_π-2. No PID cuts are applied. BOT is the average of beam on times 1 & 2 (Threshold cuts: 5 μA for BCM 1 and 1 μA for BCM 2). htr1 is the "old" tracking efficiency (pass 1), while htr2 is the "new" tracking efficiency (pass 2). The final column is the number of HMS singles passing the cuts listed in Eqn. 9.

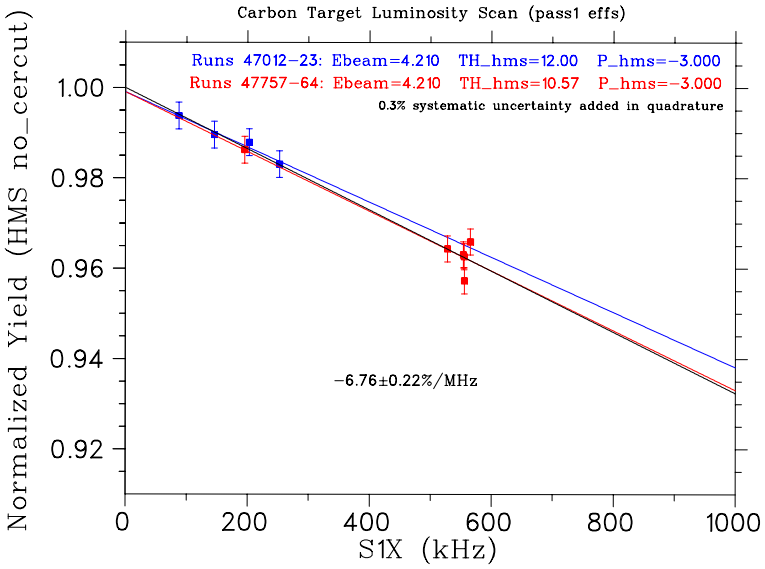

FIG. 9 Normalized yields (no PID cut) from carbon target versus HMS singles rate. The "old" tracking efficiency calculation, using a data sample where multiple track events are rejected, is better suited for higher rates ($>$ 600 kHz). Tracking efficiencies for both of the F_π-1 and F_π-2 data sets were computed using the "old" method and corrected with the linear rate dependent function presented here.

in the figure) and normalized to unity at zero rate. The two data sets, thus normalized, were then fit together, yielding the black curve.

The observed rate dependence suggests that the "old" tracking efficiencies should be corrected in the following manner

$$htr\_corrected = htr\_old \times (1 - S1Xrate(kHz) * 6.76236 \times 10^{-5}). \quad (10)$$

This correction nearly accounts for the difference between the "old" (htr1) and "new" (htr2) effi-

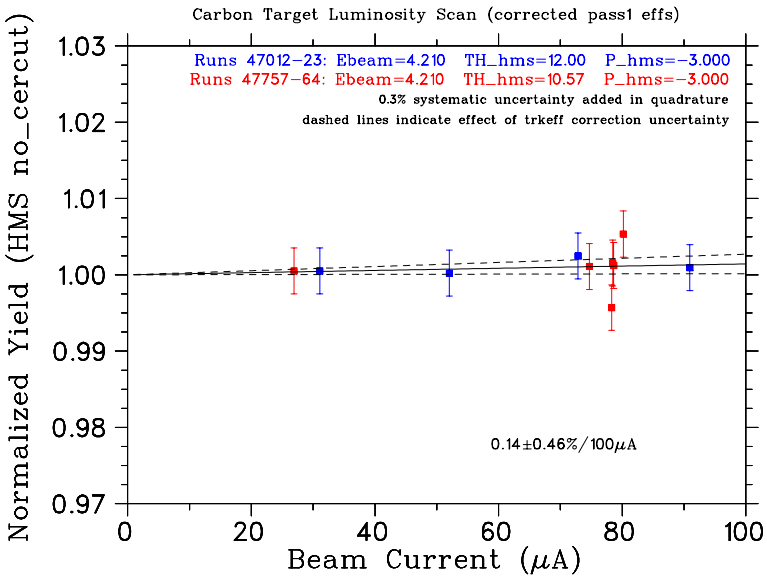

FIG. 10 Carbon yields, after the "old" tracking efficiencies are corrected according to Eqn. 10 versus current, confirming that the applied correction yields consistent results for both kinematic settings. The dashed lines were obtained by applying to the data a tracking efficiency correction raised/lowered by 1σ (Fig. 9), and refitting the current dependence.

ciencies listed for the second kinematic setting in Table I, but yields only a small correction to the "old" tracking efficiencies listed for the first kinematic setting.

Normalized carbon yields, after the "old" tracking efficiencies are corrected according to Eqn. 10, are plotted versus current in Fig. 10. This confirms that the applied correction eliminates spurious rate-dependent effects for both kinematic settings, even though they are taken at significantly different combinations of rates and currents.

To summarize, the tracking efficiencies plotted in Fig. 7 were corrected for the tracking efficiency dependence upon rate shown in Fig. 9 and applied to the normalized π^- pion yields (for both F_π-1 and F_π-2). Because of the higher rates encountered in π^- running, the HMS tracking uncertainties were assumed to be 50% larger than for π^+ running.

D. Cryotarget Boiling Correction

When the electron beam hits the liquid target, it produces a large power deposition per unit target area and as a result induces localized density fluctuations referred to as "target boiling". In order to reduce these fluctuations, the beam was rastered over a small area rather than localizing it at one point on the target. The target boiling effect can be measured by comparing the yields at fixed kinematics and varying beam current. During both experiments (F_π-1 and F_π-2), dedicated

luminosity elastic runs were taken for both liquid targets (Hydrogen and Deuterium). The two experiments used cryotargets with significantly different geometries, leading to very different boiling effects.

Run	Q_{tot}	hELLO	hS1X	BOT	PS1	htr1	htr2	cpult	hele	S1.5	S2	S99
Q^2=2.45, low ϵ, $E_e = 4.21$ GeV, $\theta_{HMS} = 10.54$												
47190	35632	593645749	759588827	1032.5	1978.1	0.9658	0.8383	0.9047	0.9589	2834	2999	150861
47191	21863	370444977	477096355	1115.5	596.3	0.9734	0.8528	0.9170	0.9765	6577	6926	327205
47192	10301	176604087	228444444	1089.5	299.1	0.9790	0.8636	0.9347	0.9886	6620	6990	323435
47241	27317	454374146	581377706	809.5	989.2	0.9656	0.8351	0.8788	0.9592	4215	4478	225052
47242	17066	284001092	363506739	530.5	989.4	0.9656	0.8372	0.8800	0.9600	2633	2768	141946
47243	15933	269682797	347254506	828.5	298.2	0.9732	0.8518	0.8671	0.9769	8872	9435	451950
47244	12196	206390831	265833195	632.5	298.2	0.9734	0.8526	0.8671	0.9768	6898	7294	346316
47245	6118	104824677	135564178	661.5	99.7	0.9792	0.8633	0.8435	0.9890	10561	11098	521854
47246	5437	93131752	120435159	578.5	99.7	0.9790	0.8621	0.8403	0.9888	9214	9722	460107
Q^2=2.45, low ϵ, $E_e = 4.21$ GeV, $\theta_{HMS} = 12.21$												
47266	56228	431953502	559403421	1134.5	992.9	0.9718	0.8599	0.9006	0.9734	4611	4876	234392
47267	32848	255082402	331707652	1114.5	398.3	0.9766	0.8704	0.9163	0.9840	7211	7597	357745
47296	10513	82800190	108090906	1132.5	99.9	0.9824	0.8809	0.9234	0.9950	9913	10298	475933
47297	49966	383049896	494990723	921.5	991.4	0.9697	0.8552	0.8743	0.9689	3976	4195	201027
Q^2=2.45, high ϵ, $E_e = 5.25$ GeV, $\theta_{HMS} = 10.61$												
47480	9204	65677147	106143067	955.8	149.8	0.9802	0.8615	0.8848	0.9945	37161	37467	256839
47481	3327	23751902	38382157	349.0	99.8	0.9802	0.8598	0.8425	0.9945	19019	19187	132571
47483	38898	272602333	435706188	806.5	992.1	0.9697	0.8397	0.7671	0.9723	18521	18793	133363
Q^2=2.45, high ϵ, $E_e = 5.25$ GeV, $\theta_{HMS} = 16.61$												
47510	65033	48592122	139812146	912.5	59.9	0.9784	0.8785	0.7819	0.9958	54175	54716	442817
47511	14012	10469724	30143430	194.5	59.9	0.9751	0.8746	0.7815	0.9958	11706	11820	95212

TABLE II Singles data taken with SCIN-3/4 HMS trigger during F_π-2 π^- running. No PID cuts are applied. BOT is the average of beam on times 1 & 2 (Threshold cuts: 5 μA for BCM 1 and 1 μA for BCM 2). htr1 is the "old" tracking efficiency (pass1), while htr2 is the "new" tracking efficiency (pass2). The htr1 tracking efficiency is subsequently corrected by Eqn. 10. The final column (S99) is the number of HMS singles events passing the cuts listed in Eqn. 11, while S1.5 and S2 have in addition cuts of $hcer\_npe < 1.5$ and $hcer\_npe < 2$ applied.

The F_π-2 cryotarget uses the "tuna can" geometry which is expected to have boiling corrections $< 1\%$ (8). However, the correction determined in Ref. (8) was determined with the "new" tracking efficiencies. To ensure that the appropriate correction is applied when "corrected old" tracking efficiencies are used, this study was repeated, using the ^{2}H data taken with SCIN-3/4 trigger to also determine the Cerenkov blocking correction. Dedicated runs with a wide variety of electron beam currents were taken for all π^- kinematic settings except Q^2=2.45, high ϵ, $E_e = 5.25$ GeV, $\theta_{HMS} = 13.61$.

Cuts of

$$abs(hsdelta) < 8.0 \qquad abs(hsxptar) < 0.09 \qquad abs(hsyptar) < 0.055 \tag{11}$$

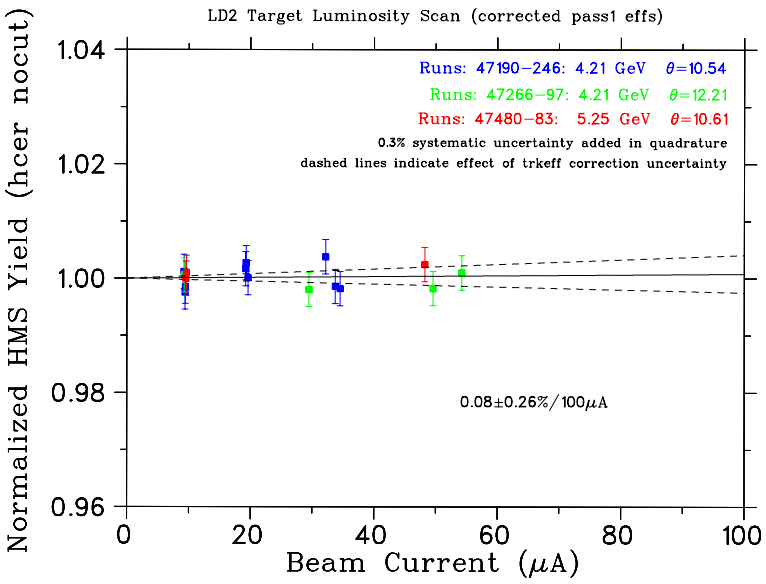

FIG. 11 Normalized HMS singles yields from F_π-2 ^{2}H π^- production data taken with SCIN-3/4 trigger obtained to also determine the Cerenkov blocking correction, plotted as a function of beam current. The dashed lines were obtained by applying to the data a tracking efficiency correction raised/lowered by 1σ n(Fig. 9), and refitting the current dependence.

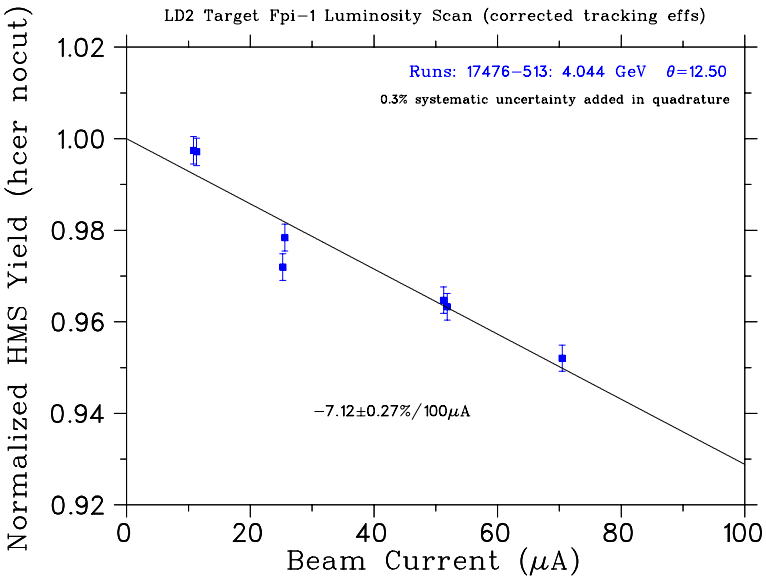

FIG. 12 Normalized HMS yields from F_π-1 ^{2}H elastics data taken with electron trigger plotted as a function of beam current.

were applied to ntuples from each of these runs, resulting in the data tabulated in Table II. The "old" tracking efficiencies (htr1 in the table) were subsequently corrected via Eqn. 11. The normalized pion yield was calculated for each run according to

$$N_{yields} = \frac{N_{sing} * PS1 + N_{coin}}{Q_{el} * El_{dt} * CPU_{dt} * Trk_{eff}}. \quad (12)$$

N_{sing} is the column labeled S99 (no Cerenkov cut) in the table. N_{coin} is the corresponding number of coincidences obtained by the same analysis, corrected for the SOS electronic live time. [For brevity, the coincidence data (C99) is not listed in the table.]

The normalized yields are plotted versus current in Fig. 11. The error bars include statistical uncertainties and an estimated systematic uncertainty of 0.3% added in quadrature. Data from the three kinematic settings were separately fit versus current and normalized to unity at zero current. The three data sets, thus normalized, were then fit together, yielding the black curve. The observed current dependence suggests that no correction should be applied, which is similar to the conclusion reached in Ref. (8), where a $<1\%/100\mu$A correction was determined with "new" tracking efficiencies.

Run	Q_{tot}	hS1X	BOT	PS1	htr	cpult	hele	SING
$E_e = 4.044$ GeV, $\theta_{HMS} = 12.50$, $P_{HMS} = -3.670$								
17476	4381	39912098	387.5	50	0.9816	0.5432	0.9983	241548
17481	7346	67005769	680.1	50	0.9818	0.5551	0.9984	414269
17487	6182	54761791	241.6	200	0.9763	0.6877	0.9964	104189
17488	23038	198857869	912.3	200	0.9762	0.6905	0.9963	387456
17491	69286	594124739	1351.4	500	0.9658	0.7335	0.9934	477416
17511	40311	345624687	777.5	300	0.9662	0.6196	0.9937	390612
17513	73205	613217684	1039.2	600	0.9569	0.6792	0.9913	375792

TABLE III HMS elastics luminosity study data taken during F_π-1. No PID cuts are applied. htr is the "old" tracking efficiency, which is subsequently corrected by Eqn. 10. The final column is the number of HMS singles events passing the cuts listed in Eqn. 9.

F_π-1 used the so-called "soda can" targets, which require significantly larger boiling corrections. The magnitude of this correction is sensitive to the rate-dependent correction applied to the HMS tracking efficiencies. The cuts listed in Eqn. 9 were applied to ntuples from each of these runs, resulting in the data tabulated in Table III. The "old" tracking efficiencies were corrected via Eqn. 11 and normalized yields calculated according to Eqn. 8. They are plotted versus current in Fig. 12. The error bars include statistical uncertainties and an estimated systematic uncertainty of 0.3% added in quadrature. Data were fit versus current and normalized to unity at zero current, yielding the black curve. The observed current dependence yields a ^{2}H target density correction of $(7.11578\times10^{-4})/\mu$A. This is somewhat larger than the $(1.15\pm0.31\%)/100\mu$A correction determined for a nearly identical ^{2}H cell in Ref. (9), but is consistent with the $(6 \pm 1\%)/100\mu$A correction determined for the F_π-1 ^{1}H cell in Ref. (6).

The fact that these target boiling corrections are consistent with previous studies supports the validity of the tracking efficiency corrections determined from the carbon luminosity studies without PID cut applied.

E. HMS Cerenkov Blocking Correction

The HMS threshold gas Cerenkov detector is used to ensure good e^-/π^- separation. In both F_π-1 and F_π-2, the HMS gas Cerenkov detector was used as a veto in the trigger for π^- runs to avoid high DAQ deadtime due to large e^- rates in the HMS. The effective gas Cerenkov thresholds used in the hardware veto are similar for both experiments. Since the actual veto threshold varies slightly from run to run due to PMT gain variations at high rates, slightly more restrictive software thresholds of were applied in the data analysis. Additionally in the F_π-2 experiment, an Aerogel Cerenkov detector was used for separating protons and π^+ for central momenta above 3 GeV/c.

The loss of pions due to Cerenkov blocking is due to electrons passing through the gas Cerenkov within ≈ 100 ns after a pion has traversed the detector, resulting in a mis-identification of the pion event as an electron and being eliminated by the analysis cuts applied. Thus, the correct estimation of the gas Cerenkov blocking correction is essential in extracting the π^- cross section and is implicit in the final estimation of π^-/π^+ ratios of separated response functions. A variety of studies were performed to determine the corrections that should be applied to both experiments.

1. F_π-2 TDC Studies

Fig. 23 shows multi-hit TDC spectra of the Cerenkov signal into the HMS trigger for two π^- SCIN-3/4 runs. The TDC is started by the HMS pretrigger signal and can be stopped multiple times by the retimed (i.e. delayed and discriminated) Cerenkov signal. The main peak corresponds corresponds to signals (primarily electrons) that result in the trigger, starting the TDC. Events not associated with the original trigger (other electrons, or pions that are mis-identified as electrons due to Cerenkov blocking) appear as additional events to the left and right of the main electron peak. The second peak to the right is due to a second electron arriving within the timing window, but after the discriminator "dead window" of $\sim$40 ns (caused by the length of the discriminator pulse). The backgrounds to the left and right of the two peaks are due to earlier and later electrons, while the tail extending to 410 ns is due to pedestal noise that crosses the discriminator threshold. The peak at channel 4096 is the accumulation of very late TDC stops, while zeros correspond to electrons (or pions) that did not give a stop.

The features of the TDC spectra were investigated for a variety of SCIN-3/4 π^- runs, for HMS singles rates up to $\sim$600 kHz. As indicated by the differences between the low rate and high rate runs plotted in Fig. 13, the main peak to pedestal ratio degrades with increasing rate, and the second peak to first peak ratio gets larger. The growth of the second peak relative to the first peak

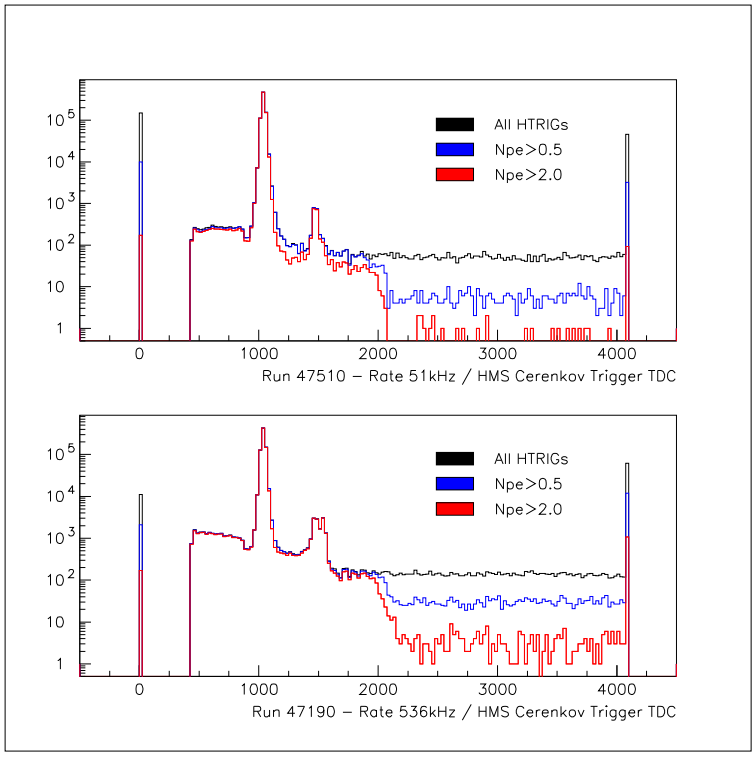

FIG. 13 TDC spectra of the Cerenkov signal into the HMS trigger for two π^- runs where the HMS trigger was SCIN-3/4. A series of cuts are placed on the number of Cerenkov photoelectrons to select "electron" events. The TDC scale is 100 ps/chan.

was confirmed to have a $\tau = 37 \pm 1$ns time constant, which is consistent with the expected TDC deadtime as indicated by the spacing between the main and second peaks.

We also confirmed that the basic features of the TDC spectra are the same for HMS singles and HMS+SOS coincidences. Fig. 14 shows this for a representative run. While the structure of the second peak is a bit different for reasons which we do not completely understand, the pedestal width and peak locations are the same in both cases. This lends confidence that any Cerenkov blocking correction determined from HMS singles data (due to smaller statistical uncertainties) should be applicable to the coincidence data as well.

While the events to the left of the 'notch' next to the main peak correspond to early electrons passing through the detector before the electrons associated with the trigger (already addressed in the coincidence time blocking correction), events to the right of the main peak correspond to electrons traversing the detector after the original trigger electrons, and the pedestal immediately beneath the main peak is due to concurrent electrons within the TDC deadtime. The concurrent and later events contribute to Cerenkov blocking which must be corrected for. The time from the notch to the left of the main peak (Chan 900) to the edge of the plateau (Chan 2050) indicates an

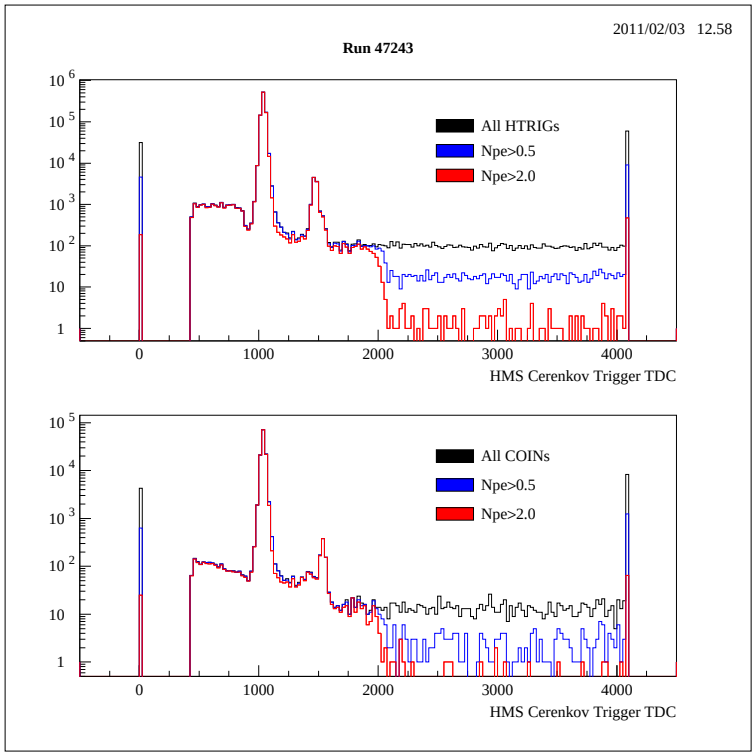

FIG. 14 Cerenkov trigger TDC for π^- run 47243, where the HMS trigger was SCIN-3/4. The mean HMS rate for this run, as computed from the ELLO scaler is 325 kHz. The top panel is the TDC spectrum for HMS singles events, while the bottom panel is for coincidence events. The TDC scale is 100 ps/chan.

effective Cerenkov TDC gate width of approximately 116 ns.

Finally, five pairs of π^- runs were identified where for each pair the beam and rate conditions were identical but the HMS trigger conditions were different (see Table IV). The TDC spectra for one of these pairs is shown in Fig. 15. While one should expect the second peak to be much smaller in the π^- data run than in the SCIN-3/4 run, we are a bit surprised that it is completely absent in the data run. Perhaps the lack of a TDC deadtime effect when the first electron is vetoed causes later electron stops to be spread further to the right, instead of piled up in a second peak. The regular π^- data run (middle panel) also exhibits some structure to the left of the main peak but otherwise the features are consistent with our expectations. The ratio of zeros to main peak counts is much greater in the π^- data run, which is consistent with the zeros being primarily pions and the main peak being electrons. The normalized difference of the two runs (bottom panel) indicates that the Cerenkov trigger is about 90% efficient at vetoing electrons.

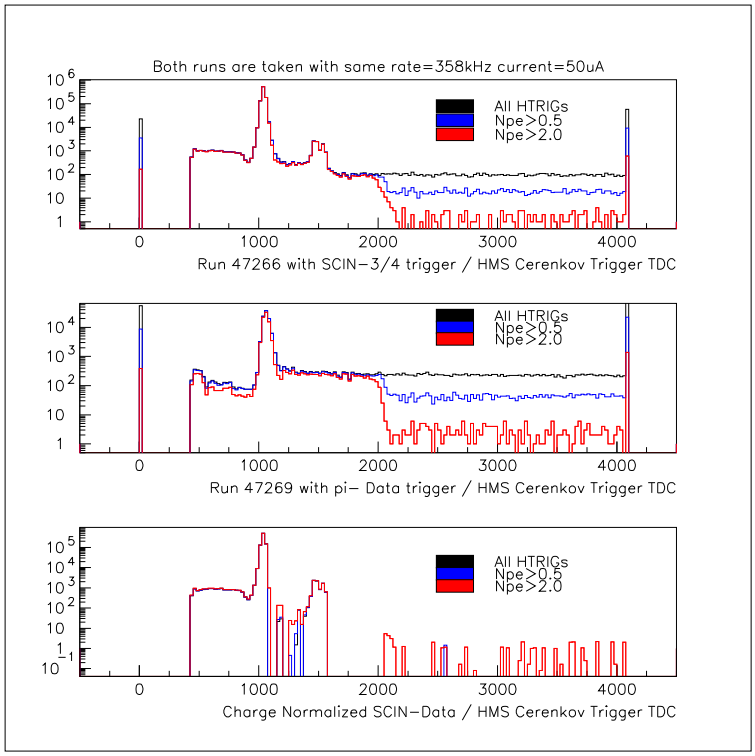

FIG. 15 Cerenkov trigger TDC for two π^- runs taken under identical beam current and singles rate conditions, but different HMS trigger conditions. The only other differences between these runs are the singles prescale factor and the CPU livetime. The bottom panel is their difference, where the data run has been normalized by charge, cpult and PS1 to the SCIN-3/4 run and then subtracted. The TDC scale is 100 ps/chan.

Run	Q_{tot}	hELLO	hS1X	BOT	PS1	htr1	htr2	cpult	hele	S1.5	S2	C1.5	C2
Q^2=2.45, low ϵ, E_e = 4.21 GeV, θ_{HMS} = 10.54													
47190	356312	593645749	759588827	1032.5	1978.1	0.9311	0.3590	0.9047	0.9589	2046	2071	3894	3941
47193	117729	1951678625	2497749072	3400.5	2994.4	0.9299	0.3585	0.9851	0.9941	4899	4963	13964	14194
Q^2=2.45, low ϵ, E_e = 4.21 GeV, θ_{HMS} = 12.21													
47266	56228	431953502	559403421	1134.5	992.9	0.9286	0.4008	0.9006	0.9734	3314	3335	4227	4264
47269	169246	1301200129	1684928207	3587.5	2996.1	0.9324	0.4043	0.9874	0.9965	3687	3720	14577	14746
Q^2=2.45, low ϵ, E_e = 4.21 GeV, θ_{HMS} = 12.21													
47297	49966	383049896	494990723	921.5	991.4	0.9326	0.4078	0.8743	0.9689	3070	3094	4600	4731
47298	166228	1274314538	1646468086	2986.5	3993.8	0.9333	0.4032	0.9840	0.9958	2776	2799	16838	17017
Q^2=2.45, high ϵ, E_e = 5.25 GeV, θ_{HMS} = 10.61													
47483	38898	272602333	435706188	806.5	992.1	0.9667	0.7294	0.7671	0.9723	16075	16188	37391	37645
47477	137020	959986136	1533128246	2872.5	5785.6	0.9657	0.7271	0.9397	0.9927	11619	11704	156783	158043
Q^2=2.45, high ϵ, E_e = 5.25 GeV, θ_{HMS} = 16.61													
47510	65033	48592122	139812146	912.5	59.9	0.9641	0.7608	0.7819	0.9958	46298	46446	10983	11020
47514	251361	186978517	531086990	3510.5	699.0	0.9642	0.7672	0.9766	0.9990	18820	18879	52502	52663

TABLE IV Selected F_π-2 π^- runs taken under identical beam and rate conditions, except that the HMS trigger conditions are different. The first run of each pair is a Cerenkov veto Test Run with SCIN-3/4 HMS trigger, and the second is a regular π^- Data Run. The column quantities are as in Table II, except that C1.5, C2 indicate coincidence events with *hcer_npe* < 1.5 and *hcer_npe* < 2 cuts applied.

2. F_π-2 Singles Yield Study

The same comparison of runs with same rate but different trigger condition can also be used to determine the effective threshold of the Cerenkov trigger veto. The sample comparison shown in Fig. 16 indicates an effective veto threshold of approximately 2.5 npe. Because PMT gain variations and pile-up effects will cause the actual veto threshold to vary with rate, a slightly more restrictive software threshold of $hcer_{npe} < 2.0$ was uniformly applied in the F_π-2 data analysis.

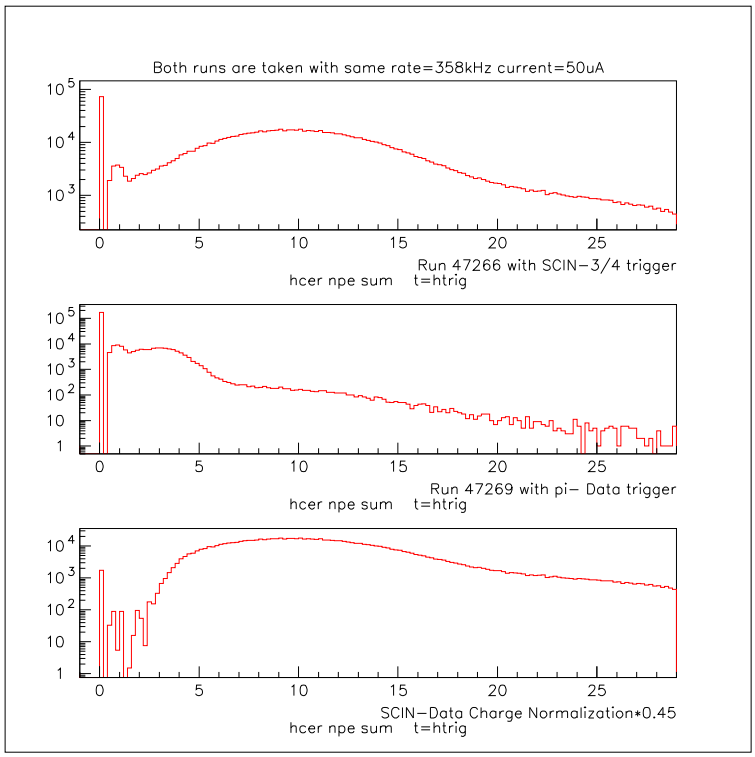

FIG. 16 Cerenkov photoelectron spectra for two π^- runs taken under identical beam current and singles rate conditions, but different HMS trigger conditions. The bottom panel is their charge normalized difference, where the normalization factor has been multiplied by 0.4 to avoid negative counts at low npe.

As already discussed in Sec. II.D, dedicated runs were taken with SCIN-3/4 trigger for a variety of electron beam currents for all F_π-2 π^- kinematic settings except Q^2=2.45, high ϵ, $E_e = 5.25$ GeV, $\theta_{HMS} = 13.61$. The purpose of these runs was to determine the Cerenkov blocking correction versus electron rate into the HMS. The data with $hcer_{npe} < 2.0$ software threshold listed in Table II were used to compute normalized pion yields in a manner similar to Eqn. 12, except that the tracking efficiency correction Eqn. 11 was applied. [Note that it might have been better to use the ELCLEAN rate in this study, however, the object is to obtain a correction which can be applied to both experiments and ELLO is the closest equivalent scaler which is available in F_π-1.]

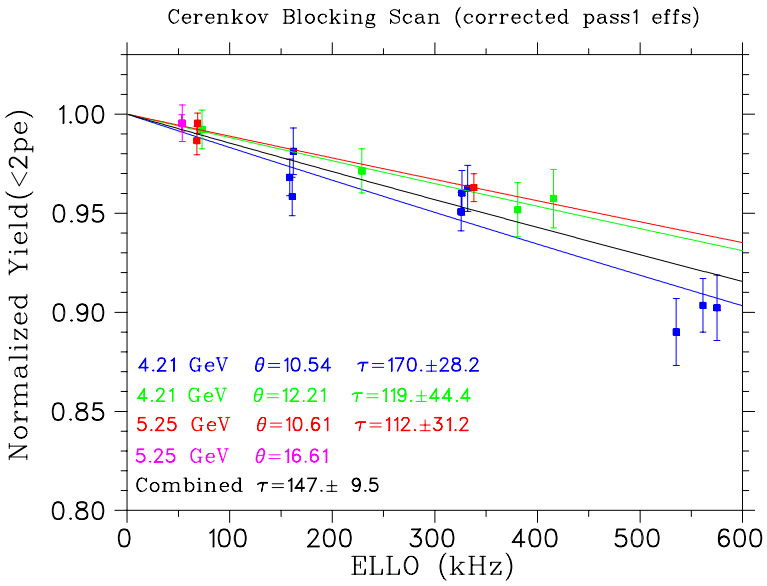

FIG. 17 Normalized experimental yields as a function of HMS singles rate, for data with SCIN-3/4 HMS trigger, with a $N_{p.e.} > 2.0$ Cerenkov particle identification cut applied. The tracking efficiency and cryotarget boiling corrections discussed in Secs.II.C.2,II.D are applied. The colored lines are fits of the form $Y = Ae^{-R\tau}$ for each kinematic setting separately. The black line is a combined fit to all of the data, as explained in the text.

To determine whether the yields for the different sets of kinematics exhibit similar rate dependencies, the three sets spanning a large range of rates were fit to functions of the form $Y = A^{-R\tau}$, where both A and τ were free parameters. Although A introduces an additional free parameter to the fit, this allows τ to be extracted for each set without being sensitive to the normalization of the 'low rate yield'. The normalized yields versus rate, and the fit τ values are shown in Fig. 17. The obtained effective gate widths are reasonably independent of kinematic setting. Because the runs at Q^2=2.45, high ϵ, $E_e = 5.25$ GeV, $\theta_{HMS} = 16.61$ are only at low rates, that τ value is not shown.

Two of the three τ_{eff} values have nearly same the values, while the third is 1.5σ larger. Additional studies were performed to see if the larger τ value could due to a different π/e ratio at this setting compared to the others. The π/e ratio was found to depend upon incident beam energy, and was nearly insensitive to spectrometer rate and angle, so it could not be the cause of the discrepancy. We conclude the three τ values are consistent within normal statistical fluctuation, and that other factors which could affect the conclusions are reasonably well under control. Since they are consistent, a combined fit of all the data was made. In this case, the three data sets spanning wide ranges of rates were independently normalized to unity at zero rate, effectively removing the cross section variation with kinematics. The $E_e = 5.25$ GeV, $\theta_{HMS} = 16.61$ setting

was then normalized to the lowest rate run of the $E_e = 5.25$ GeV, $\theta_{HMS} = 10.61$ setting. The combined fit to the renormalized data is shown by the black line in Fig. 17. The combined fit unavoidably depends on the renormalization constants chosen for the four kinematic settings, but the methodology employed does not allow too much arbitrary judgment.

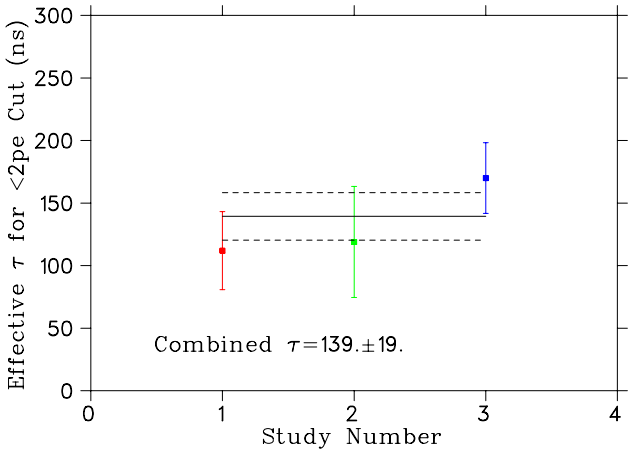

FIG. 18 Effective Cerenkov gate widths for the $hcer_{npe} < 2.0$ cut used in the F_π-2 data analysis, color coded according to the fits versus rate in Fig. 17. The black line is the error-weighted average, while the dashed lines indicate the uncertainty.

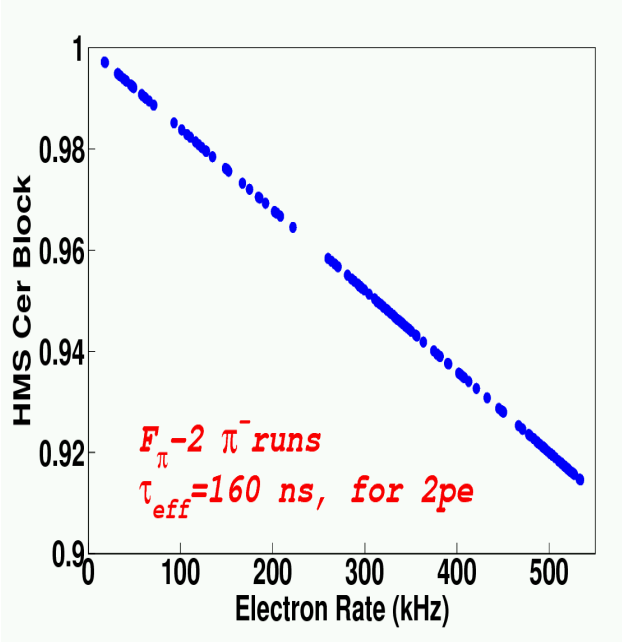

FIG. 19 F_π-2 HMS Cerenkov blocking correction $\delta_{CCblock}$ plotted as a function of the HMS singles rate. At high rates (≈600 Hz) the correction is at the level of 9%. **THIS FIGURE IS NOT YET UPDATED FOR THE NEW BLOCKING CORRECTION.**

The Cerenkov blocking τ_{eff} value and its uncertainty was estimated from the fits to the three kinematic settings shown in Fig. 17. Note that these fits depend sensitively upon the tracking

efficiency and cryotarget boiling corrections used. Taking into account the respective uncertainties in these fits yields a central value of 139 ± 19 ns.

Since this τ value was determined with singles events, it needs to be adjusted to yield the effective gate width for coincidence events. As discussed in Sec. II.E.1, the region to the left of the main peak in Figs.13-15 corresponds to early electrons passing through the detector before the electrons associated with the trigger, already addressed in the coincidence time blocking correction. The correction factor is the ratio of the time from the notch to the left of the main peak (Chan 900) to the right edge of the plateau (Chan 2050), divided by the time of the full distribution (Chan 425 to Chan 2050),

$$\frac{116.4 \pm 6.3 \text{ ns}}{162.9 \text{ ns}} = 0.714 \pm 0.039. \tag{13}$$

Multiplication by this factor gives $\tau_{eff} = 99.2 \pm 19$ ns, which is used to compute the Cerenkov blocking correction

$$\delta_{CCblock} = e^{-ELLOrate*\tau_{eff}}. \tag{14}$$

appropriate for the F_π-2 π^- analysis, shown as a function of the HMS singles rate in Fig. 19.

3. Cerenkov Blocking Correction for F_π-1 Data

Open trigger data at different electron rates were unfortunately not taken during the F_π-1 experiment, so the Cerenkov blocking correction cannot be directly determined for those data. We therefore modify the Cerenkov blocking correction determined from F_π-2 data for use in the F_π-1 analysis according to the following procedure.

Fig. 20 shows a HMS Cerenkov photoelectron histogram for a carbon elastics run taken at the very beginning of F_π-1, immediately before the first π data run. It indicates that the effective veto threshold in the F_π-1 experiment is slightly lower than that used in F_π-2. Therefore, a slightly more restrictive software threshold of $hcer_{npe} < 1.5$ was applied in the analysis of the F_π-1 data. The figure also indicates that the Cerenkov veto is about 80% efficient for this run. Very few timing checks were performed after the initial experimental setup, and our investigations indicate that the Cerenkov veto efficiency varied with kinematic setting during the F_π-1 experiment.

We therefore reanalyzed the F_π-2 dedicated π^- runs with SCIN-3/4 trigger, except that a $N_{p.e.} > 1.5$ Cerenkov particle identification appropriate to the F_π-1 analysis was applied, and obtained the results shown in Figs. 21,22. Taking into account the respective uncertainty in these

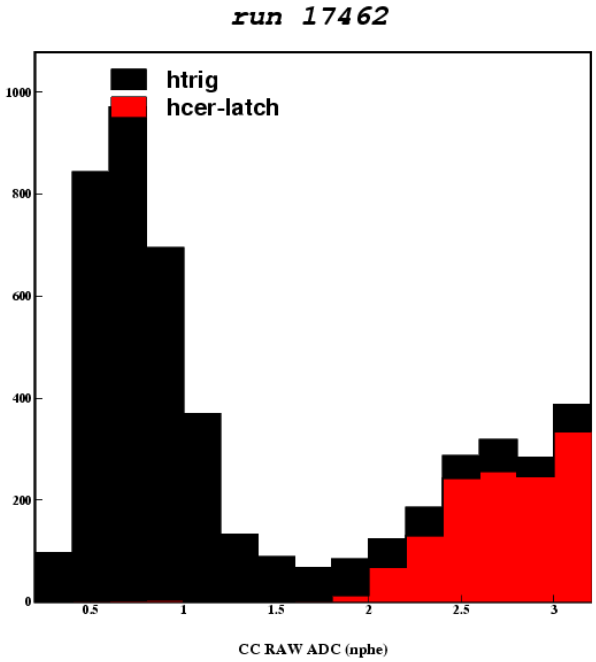

FIG. 20 A summed photoelectron histogram from the HMS Cerenkov for a representative F_π-1 carbon elastics run, $^{nat}C(e,e')$. The Cerenkov veto is not in the trigger; those events which would have most likely been vetoed (as determined from a nonzero Cerenkov trigger TDC value) are indicated in red. The effective veto threshold appears to be at about 2 photoelectrons.

three fits yields a central value of $\tau = 162 \pm 19$ ns, which is then corrected by Eqn. 13 to give $\tau = 115.7 \pm 20$ ns.

Finally, we used the TDC timing information from the only F_π-1 "open trigger" SCIN-3/4 run taken just before the main data taking to estimate the scaling with respect to the F_π-2 timing information. As shown in Fig. 23, the TDC timing window used during F_π-1 is wider than in F_π-2. Comparing the time from the notch to the left of the main to the edge of the plateau in the F_π-2 spectrum (116 ± 6 ns) to the equivalent features in the the F_π-1 spectrum (138 ± 6 ns), indicates a scale factor of 1.19 ± 0.084.

Application of this scale factor to the τ value determined from the F_π-2 data gives an effective τ value for the F_π-1 analysis of $\tau_{eff} = 137.7 \pm 26$ ns. This value is used to compute the CC blocking corrections used for the F_π-1 data normalization, shown as a function of the electron rate in Fig. 24.

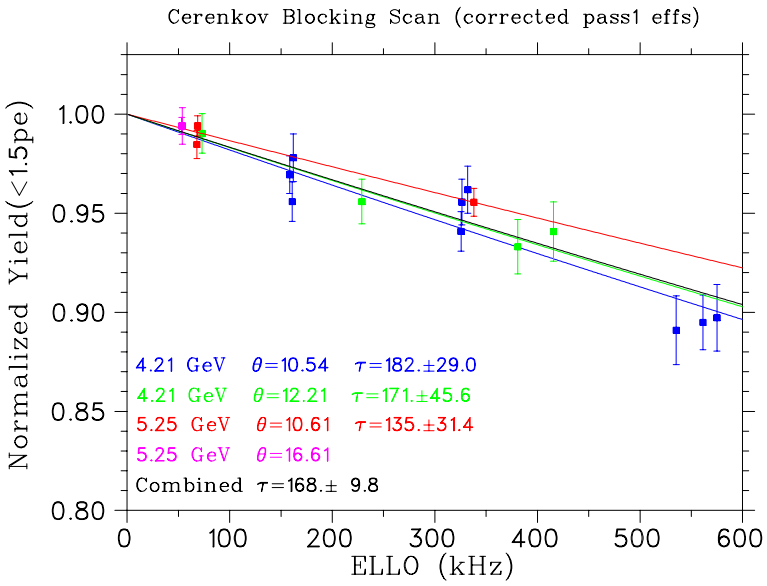

FIG. 21 The data are the same as in Fig. 17, except that a $N_{p.e.} > 1.5$ Cerenkov particle identification appropriate to the F_π-1 analysis is applied.

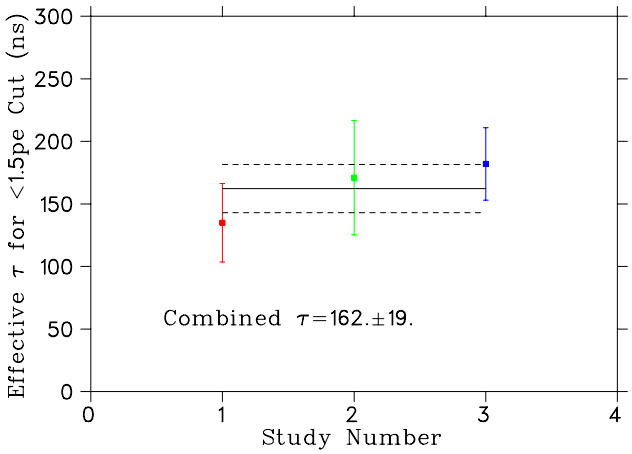

FIG. 22 Effective Cerenkov gate widths determined from F_π-2 data, but with a $hcer_{npe} < 1p5$ cut appropriate for the F_π-1 data analysis.

F. F_π-2 Yield Ratio Study

The five pairs of π^- runs identified in Table IV, where for each pair the beam and rate conditions were identical but the HMS trigger conditions different, can be used to probe additional rate dependent effects. The ratios of normalized yields

$$R = \frac{N_{\pi^-\_run\_with\_veto}}{N_{\pi^-\_run\_without\_veto}} \tag{15}$$

were thus formed, using the $N_{p.e.} < 2.0$ data (columns S2 and C2) in Table IV. As indicated from the values in the table, the uncertainty in the tracking efficiency and target boiling corrections

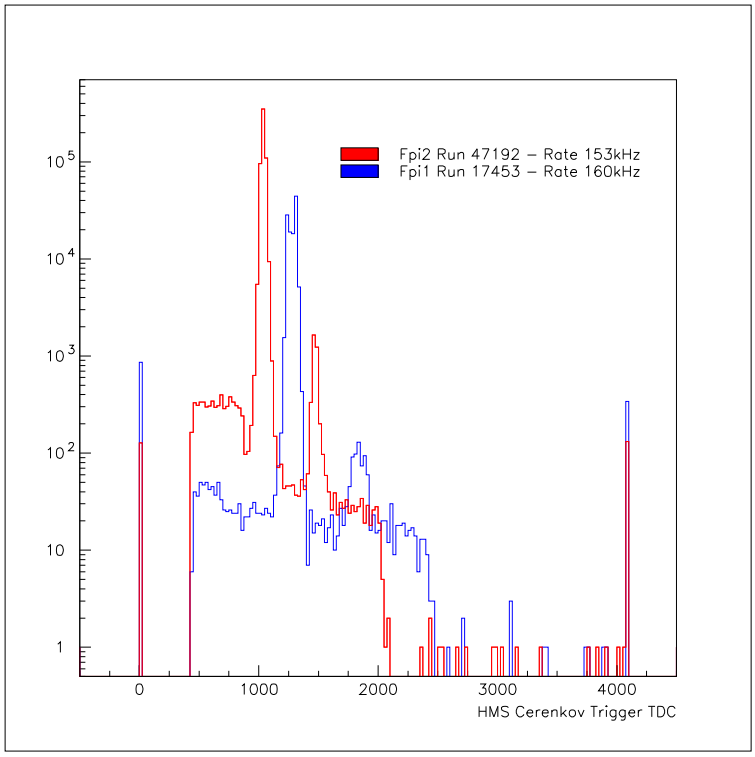

FIG. 23 Cerenkov Trigger TDC histogram for the one F_π-1 π^- run with SCIN-3/4 trigger (blue), compared to a F_π-2 SCIN-3/4 run at similar rate (red). HMS singles events, subject to a $N_{p.e.} > 2.0$ Cerenkov cut, are used in both spectra. The TDC scale is 100 ps/chan.

cancel in the formation of the ratio, depending only on the knowledge of the cpu livetimes and prescale factors. These ratios are plotted versus rate in Fig. 25. The effective gate width determined from this study, determined from a fit which is constrained to unity at zero rate, is $\tau = 91 \pm 22$ ns, while a fit without this constraint gives $\tau = 37 \pm 37$ ns. This indicates a small residual rate dependence beyond those taken into account in the analysis. Since the prescale factors should be known, it is likely the issue is due to the cpu livetime. It is sometimes an issue that heavily prescaled singles events encounter a different cpu livetime than coincidence events. It seems likely that the residual rate dependence of the singles ratios shown in Fig. 25 is due to this issue. Without accurate information on the singles cpu livetime we cannot proceed further. We note that studies of this nature could be a valuable tool in our planned 12 GeV experiments, and we should aim to acquire better data to allow a more complete study in the future.

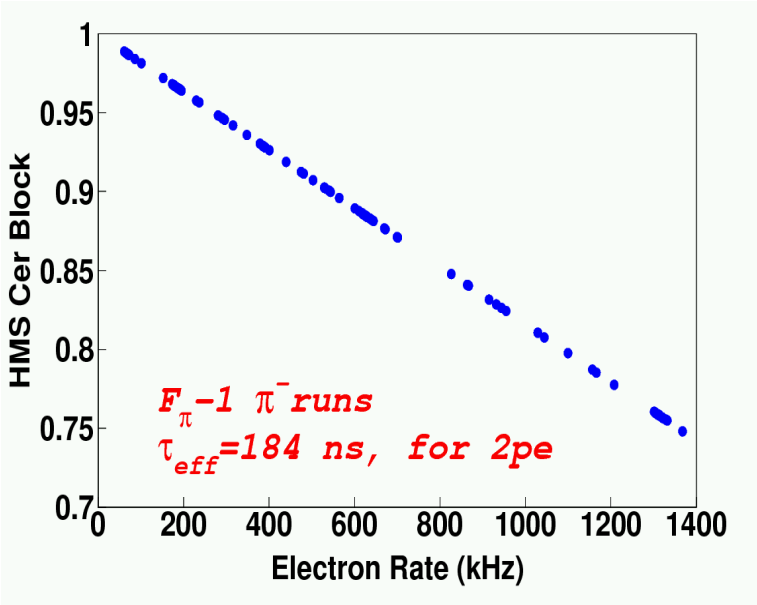

FIG. 24 F_π-1 HMS Cerenkov blocking correction $\delta_{CCblock}$ plotted as a function of the HMS singles rate. At high rates (≈1.4 MHz), the correction is at the level of 25%. **THIS FIGURE IS NOT YET UPDATED FOR THE NEW BLOCKING CORRECTION!**

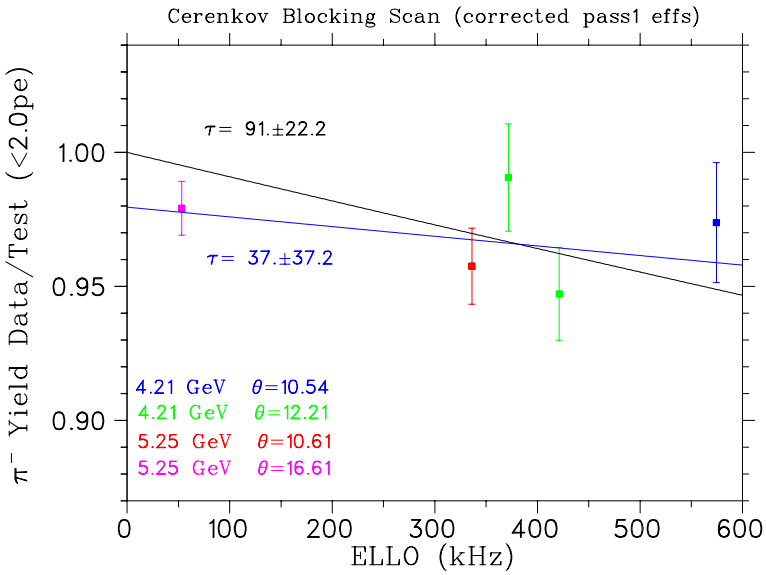

FIG. 25 Yield ratios versus HMS singles rate for π^- runs where the Cerenkov veto was included in the HMS trigger, divided by the corresponding run at same current and rate where the HMS trigger was SCIN-3/4. A 1% systematic uncertainty has been added in quadrature to all ratio error bars.

G. HMS Beta Cut Correction

In the main analysis package, β is the velocity of the detected charged particle determined from the time of flight between the two scintillator hodoscopes in the detector stack. The coincidence time spectrum at low β (Fig. 26) displays a "tail" due to pions undergoing nuclear interactions in the scintillators, Cerenkov detector material, and in the case of F_π-2 experiment the Aerogel Cerenkov detector material which was absent during F_π-1. These scattered pions have a larger time of flight. There are also events with $\beta = 0$, which means that no hits in the relevant scintillators were found when projecting the reconstructed track to the hodoscopes.

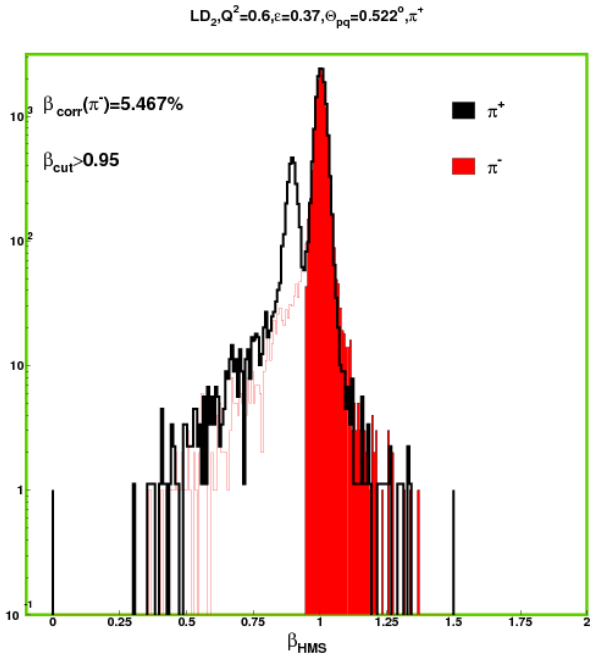

FIG. 26 β_{HMS} spectrum for the π^- channel (red thin line) and the π^+ channel (black thick line), scaled with respect to each other, and overlapped with the β_{HMS} region defined by the $\beta > 0.95$ cut (solid area) for one of the F_π-1 kinematic settings.

Due to the fact that the Aerogel Cerenkov detector was not yet in existence at the time of the F_π-1 experiment, it was not possible to cleanly eliminate the proton background which contaminated the π^+ data set. In order to reduce the proton contamination of π^+ data set, we applied a beta

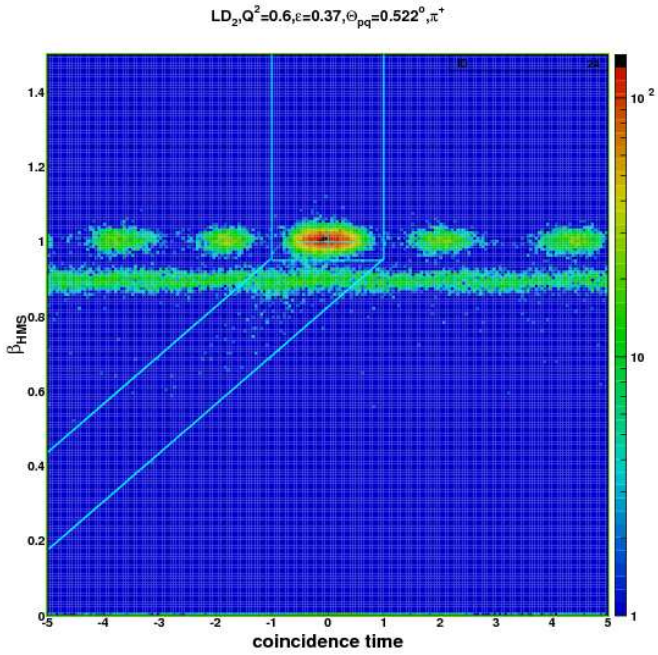

FIG. 27 Coincidence timing spectrum plotted versus β for the F_π-1 data set. The solid lines indicate the cuts applied on both variables in order to select "good electrons" as well as to compute the β cut correction.

Kin	Q^2	ϵ	$\theta_{pq}[deg]$	β_{cut} corr. [%]
1	0.6	0.37	0.5	5.46
2	0.6	0.37	4	5.42
3	0.6	0.74	0	4.81
4	0.75	0.43	0	5.11
5	0.75	0.43	4	4.69
6	1.0	0.33	0	5.02
7	1.0	0.33	4	4.57
8	1.0	0.65	0	5.23
9	1.6	0.27	0	5.05
10	1.6	0.27	4	4.09
11	1.6	0.63	-4	5.04
12	1.6	0.63	0	4.80
13	1.6	0.63	4	4.27
Mean				4.89 ± 0.41

TABLE V β_{cut} corrections for the π^- channel for each of the 13 F_π-1 kinematic settings. Note that the correction was applied as a normalization constant for each kinematic setting separately.

cut $\beta > 0.95$, as shown in Fig. 26. The so called "beta cut correction" was defined as the ratio of the "blob" (defined by the following cuts: $-1 <$ coincidence timing < 1 and $\beta > 0.95$), and "blob" plus "tail" as shown in the Fig. 27. This correction was extracted from π^- data and applied to

both data sets (π^+ and π^-) as a normalization constant to account for the pions lost due to this cut. The β cut correction used in the final F_π-1 normalization was 4.89% with an uncertainty of 0.41% determined from the standard deviation, as indicated in Table V.

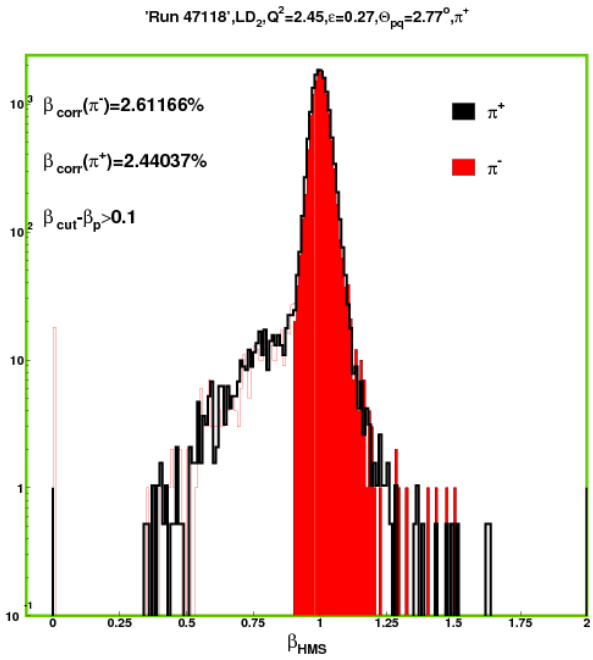

FIG. 28 β_{HMS} spectrum for π^- (red thin line) channel and π^+ (black thick line) channel, scaled with respect to each other, and overlapped with the β_{HMS} region defined by the $\beta > 0.95$ cut (solid area) for one of the F_π-2 kinematic settings.

For the F_π-2 data set, the same procedure was used, but adjusted for the presence of the Aerogel Cerenkov detector. This permitted the separation of protons from pions, leading to a much cleaner pion sample (Fig. 28). For each π^+ and π^- kinematic setting, "beta cut corrections" were extracted in the same fashion as explained earlier (see Fig. 29). The corrections are summarized in Table VI. The β cut corrections used in the final F_π-2 normalization were 2.42% with an uncertainty of 0.12% in the π^+ case, and 2.51% with an uncertainty of 0.18% in the π^- case.

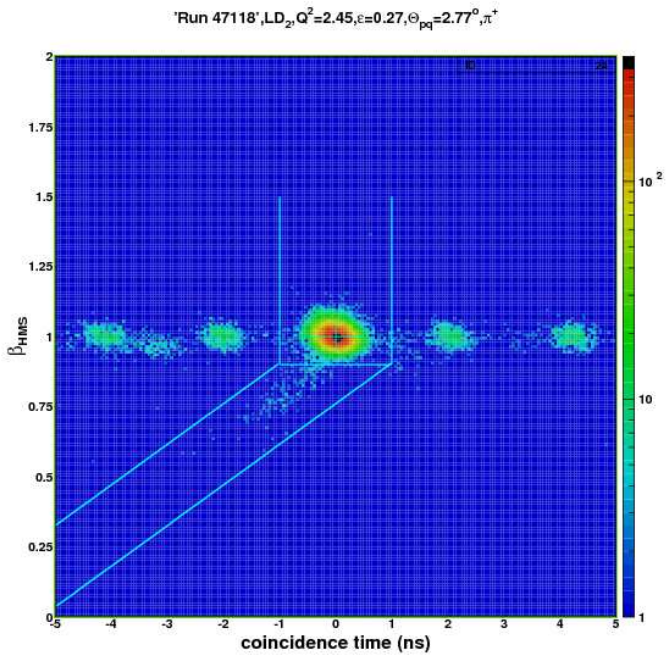

FIG. 29 Coincidence timing plotted versus the β of the detected charged particle for the F_π-2 data set. The solid lines indicate the cuts applied on both variables in order to select "good electrons" as well as to compute the β cut correction.

H. Pion Absorption in HMS

A fraction of the produced pions are lost as a result of nuclear interactions in the materials that they traverse before reaching the HMS detectors. For the pion momenta used in F_π-1,2, the dominant pion reaction types are the inelastic scattering and charge exchange processes, resulting in a deflection and loss of momentum of the pion, and the pion absorption process, resulting primarily in the emission of energetic protons and neutrons. The proportion of pions lost due to these processes must be correctly accounted for. The situation is complicated by the fact that pion absorptions in the scintillators, aerogel, and Cerenkov detector material leading to the emission of energetic protons are already included in the β efficiency correction. The pion absorption correction is intended to account for the HMS triggers which are lost due to pion interactions in materials upstream of the drift chambers, or interactions in the detector stack such as large angle deflection, or absorption processes leading to the emission of only low momentum or neutral particles.

Kin	Q^2 ϵ θ_{pq}	β_{cut} corr. [%]
π^+ Settings		
1	2.45 0.27 2.77	2.44
2	2.45 0.27 3.65	2.59
3	2.45 0.54 2.41	2.30
4	2.45 0.54 4	2.30
5	2.45 0.54 -3	2.45
Mean		2.42 ± 0.122
π^- Settings		
1	2.45 0.27 2.77	2.61
2	2.45 0.27 3.65	2.60
3	2.45 0.54 2.41	2.71
4	2.45 0.54 4	2.33
5	2.45 0.54 -3	2.31
Mean		2.51 ± 0.179

TABLE VI β_{cut} corrections for each of the F_π-2 kinematic settings.

To study the interplay between the pion absorption and β corrections, the transmission of pions from the target through to S2X was calculated and used to estimate which fractions of these end up in the various parts of the β versus coincidence time spectrum. The pion transmission for each material was calculated by making use of their known areal densities and the nuclear collision lengths λ from Ref. (10). Since these λ values are only appropriate for high energy particles, where the energy dependence is small, they were rescaled according to the energy dependence of the $\pi^+ p$ interaction. It was assumed that all pion reactions from the target to spectrometer exit window resulted in lost triggers. For the pions reacting from the drift chambers to S1, it was assumed that a fraction f_1 were lost triggers, while the remaining $1 - f_1$ were not lost, but ended up with either $\beta = 0$ (meaning no valid track was found by the tracking algorithm) or in the 'tail' (β below the cut value). Finally, for the interactions from the Cerenkov through to the first 1/4 of S2, it was assumed that fraction f_2 resulted in a low β value, while the remaining $1 - f_2$ were indistinguishable from those pions that did not undergo nuclear reactions.

To determine the fractions f_1, f_2 appropriate for the F_π-1,2 deuterium data, the following procedure was employed. The fractions of $\beta = 0$, 'tail' and 'blob' events were determined for each F_π-1 π^- setting, and for each F_π-2 π^- and π^+ setting (see Fig. 30). Since low β values could also be due to instrumental timing effects, the same proportions were also determined from representative F_π-1,2 runs with electrons in the HMS. The electron fractions were then subtracted from the pion fractions, yielding typical 'zero+tail' values of 2.2+4.0=6.2% (2.6+2.2=4.8%) for F_π-1 (F_π-2), with the remainder in the 'blob'. f_1, f_2 were then inferred by comparison of the observed 'zero+tail' values to the calculated interaction probabilities. For F_π-1, the calculation

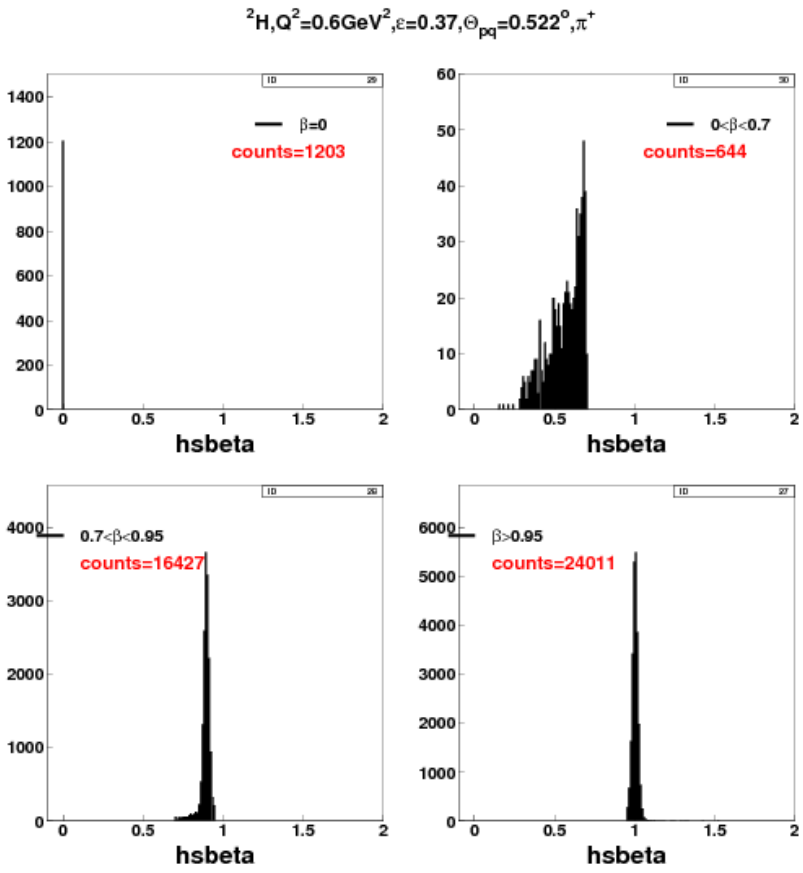

FIG. 30 HMS β spectrum for a representative π^+ run in F_π-1, showing the proportion of HMS events with $\beta = 0$, the proportions in the 'low' ($0 < \beta < 0.7$) and 'high tails' ($0.7 < \beta < 0.9$), and those in the 'blob' ($\beta > 0.9$). To avoid proton contamination due to the lack of an Aerogel Cerenkov detector in F_π-1, the higher cut value of $\beta = 0.95$ was used to define the 'blob' and 'tail' regions in the calculation of the pion absorption correction.

predicted too few zero+tail events and too many in the blob, with the closest agreement being for the assumption that none of the interacting pions resulted in lost triggers ($f_1 = 0$), and 100% of the interacting pions ended up in the 'zero+tail' ($f_2 = 1$). For F_π-2, values of f_1=30-45% and $f_2 = 75 - 100\%$ resulted in good agreement with the data.

Since the calculated interaction probability from the target to exit window was 0.55% for F_π-1,

and 0.70% for F_π-2, we estimated pion absorption corrections of $1\% \pm 1\%$ for F_π-1 and $2\% \pm 1\%$ for F_π-2. The higher F_π-2 value is mainly due to the thicker titanium spectrometer exit window and the addition of the aerogel Cerenkov in the detector stack.

I. Data Corrections Summary

Summary of F_π-1 Correction Factors	
HMS tracking efficiency	$1 - (0.0676 \pm 0.0022)$/S1Xrate(MHz)
LD_2 Cryotarget Boiling	$1 - (0.0712 \pm 0.0027)/100\mu$A
HMS Cerenkov blocking	$e^{-\mathrm{ELLOrate}*(99.2\pm19\mathrm{ns})}$
β_{cut} correction ($\pi^\pm$)	$4.89\% \pm 0.41\%$
Pion Absorption	$1\% \pm 1\%$
SOS Cerenkov efficiency	$99.92\% \pm 0.02\%$ (8)
SOS Calorimeter efficiency	$99.5\% \pm 0.1\%$ (8)
HMS Cerenkov efficiency	$99.6\% \pm 0.05\%$ (8)
Coincidence Blocking	$e^{-\mathrm{TotalPretrigrate}*(140\mathrm{ns})}$ (6)
Summary of F_π-2 Correction Factors	
HMS tracking efficiency	$1 - (0.0676 \pm 0.0022)$/S1Xrate(MHz)
LD_2 Cryotarget Boiling	No correction.
HMS Cerenkov blocking	$e^{-\mathrm{ELLOrate}*(137.7\pm26\mathrm{ns})}$
β_{cut} correction (π^-)	$2.51\% \pm 0.18\%$
β_{cut} correction (π^+)	$2.42\% \pm 0.12\%$
Pion Absorption	$2\% \pm 1\%$
SOS Cerenkov efficiency	$99.92\% \pm 0.02\%$ (8)
SOS Calorimeter efficiency	$99.5\% \pm 0.1\%$ (8)
HMS Cerenkov efficiency	$99.6\% \pm 0.05\%$ (8)
HMS Aerogel efficiency	$99.5\% \pm 0.02\%$ (8)
Coincidence Blocking	$e^{-\mathrm{SOSPretrigrate}*(92\mathrm{ns})}$ (8)

TABLE VII Summary of corrections applied to the data.